



Cooperative Path Following Control of Fixed-wing Unmanned Aerial Vehicles with Collision Avoidance

Shulong Zhao¹ · Xiangke Wang¹ · Hao Chen¹ · Yajing Wang¹

Received: 9 November 2019 / Accepted: 18 May 2020
© Springer Nature B.V. 2020

Abstract

In this paper, we propose a novel curved path following scheme for multiple fixed-wing unmanned aerial vehicles (UAVs) that can achieve coordinated curved path following and handle collision avoidance simultaneously. The proposed solution is a hybrid system that combines a path following strategy and a collision avoidance method to ensure collision-free maneuvering of a group of UAVs cooperative flight. A strategy based on a virtual structure and a kinematic model is proposed to derive the cooperative curved path following. Meanwhile, a possible collision will occur when multi-UAVs flight in the form of dense formations, or there are path intersections when the formation is changed. However, all fixed-wing vehicles need to maintain a minimum airspeed and cannot stop before the collision. Therefore, there is a need for a fast and efficient method that can be implemented online, taking into account the physical limitations of the vehicle (minimum speed, turning rate, etc.) to avoid possible collision. We employ a modified vector field histogram (VFH) method to provide real-time collision avoidance, and evasive maneuvers work only if the distance is within the conflict zone. In order to verify the proposed control scheme, dense formation flight tests of small fixed-wing UAVs were implemented.

Keywords Cooperative path following · Fixed-wing UAVs · Vector field histogram (VFH) · Collision avoidance

1 Introduction

Nowadays, fixed-wing unmanned aerial vehicles (UAVs) has been used in many military and civilian applications, such as target tracking, surveillance, traffic monitoring, environmental data collection, and geographic mapping. How to quickly and efficiently assemble together and avoid collisions in a dense formation or during formation transformation is a challenging task for multi-UAVs. It is necessary to design a strategy to guide multi-UAVs to coordinate path following while avoiding collisions with each other.

There are many methods and strategies that have been proposed for the coordinated flight and autonomous

collision avoidance of multi-UAVs [1]. The methods of the existing literatures can be divided into two categories depending on the implementation:

(1) Planning based strategies.

Global online path planning methods are widely used for multi-UAVs formation flight. Online path planning is implemented within each optimization loop, and local optimal path instructions are passed to the tracking controller by minimizing certain cost functions. By repeating this process in each loop, a valid globally optimal path will be guaranteed [2]. The most popular path planning methods include model predictive control (MPC) [3], graph search algorithm (A^* [4], D^* [5]), optimization of paths (mathematical programming [6], evolutionary [7] and particle swarm optimization (PSO) [8]) and artificial potential field (APF) [9].

The main performance of the planning algorithm is completeness, which manifests whether an available path is obtained to follow. The calculation time of most planning strategies is uncertain, so the resulting path may not be optimal. At the same time, some gradient-based optimization algorithms may be easily stacked into the local minimal value. For on-line path planning

This work is supported by National Natural Science Foundation (NNSF) of China under Grant 61973309.

✉ Shulong Zhao
xkwang@nudt.edu.cn; xiangkewang@gmail.com

¹ College of Intelligence Science and Technology, National University of Defense Technology, Changsha, 410073, People's Republic of China

algorithms, the computational performance of the on-board computer is also critical to the rapid response to unknown environments in high-speed flight situations.

(2) Control protocol based strategies.

Techniques based on control protocols typically use the model of the vehicle and the data collected from the sensors to construct zone boundaries to obtain control instructions with appropriate speed and heading. The proposed methods include sliding mode navigation [10], boundary following [11], wall following [12] and so on. The method based on the control protocol should first ensure convergence of the tracking error, and secondly, avoid collisions. However, the priority to collision avoidance is higher, and the corresponding control strategy is a dual-mode (safe mode and dangerous mode) structure.

Fixed-wing UAVs are easily subject to limitations (energy limitations and input saturation) and disturbances (wind and noise). The corresponding control protocol strategy must be proposed to solve these problems. However, in most of the literature [13–15] the vehicles are assumed to cruise at a constant speed, and this speed must be specifically selected according to the predetermined path.

In this paper, we mainly focus on the problem of multi-UAVs cooperative curved path following and collision avoidance. The desired path is expressed in Frenet-Serret coordinates, and a cooperative curved path following strategy is proposed to ensure that the vehicle converges from the initial position to the desired path. In the problem of the UAV path following, the airspeed is usually assumed to be a constant value, just to adjust the nose to the desired path. However, it is difficult to implement a cooperative path following strategy by only changing the orientation of the UAVs. In this article, we especially consider the airspeed of the vehicles being not constant, which act as additional control inputs to control the positions of the UAVs. Different from the commonly used planning-based methods, an improved vector field histogram (VFH) is proposed for efficient collision avoidance. In addition, possible collisions must be identified and automatically resolved as the vehicle approaches the path. The emergency avoidance maneuver is formed by independently changing the heading and speed of each UAV. Compared with planning strategy methods [2–4], our proposed method is more practical and can deal with uncertain factors caused by environmental wind disturbance, measurement noise or unmodeled dynamics. Compared with the control protocol method [10–12], our proposed method can more flexibly adjust the forward speed of each UAV, and realize the dual consideration of formation switching and safe flight.

This paper is organized as follows. The problem formulation and control objective are shown in Section 2.

The proposed control scheme is presented in Section 3. Section 4 describes the implemented flight experiments. The conclusion goes in Section 5.

2 Preliminaries and Problem

The problem of multi-UAVs cooperative curved path following and collision avoidance is considered. Unlike the path planning method, the desired path of the UAV is predefined by a series of waypoints. These vehicles share their current and potential locations in space, and the initial distance between them should be greater than the designed safety distance. This paper focuses on coordinated flight and collision avoidance within a formation. The relative positions of the UAVs are assumed to be known and communicated through the central control system without delay.

Since the UAV is flying at a cruising speed (15–19 m/s), the available avoidance time depends on the choice of the safety distance. It is essential to estimate the potential collision and implement emergency avoidance maneuvers in advance.

2.1 System Dynamics

A cooperative path following system consists of n fixed-wing UAVs that have the same kinematic description and no leader. Each vehicle has a propeller and four control surfaces (ailers, rudders and elevators). As [14] shows, a common dynamical model of a fixed-wing UAV can be described as

$$\begin{aligned}\dot{x}_i &= v_{gi} \cos \chi_i \\ \dot{y}_i &= v_{gi} \sin \chi_i \\ \dot{\chi}_i &= \omega_i\end{aligned}\tag{1}$$

where (x_i, y_i) indicates the position of the UAV in the earth coordinate, χ_i represents the course angle (the direction of travel relative to the earth's surface), v_{gi} represents the ground speed. Note that the variables in terms of airspeed v_a and heading angle ψ are not employed, which has the advantage of wind disturbance rejection [16].

Formally, the desired paths are defined in Frenet-Serret frame [17]. Suppose the path is described by a differentiable arc-length parameter s (Fig. 1), which indicates the distance from the any reference point $P_r = [x_r, y_r]$ on the path to the starting point P_0 ($s = 0$).

We assume that the formation of multi-UAVs has a center of the virtual structure, $P_d = (x_d, y_d)$, which moves along a predefined path L and has an angle $\chi_0 = \arctan(\dot{y}_d, \dot{x}_d)$ with respect to the inertial frame. There are n edges

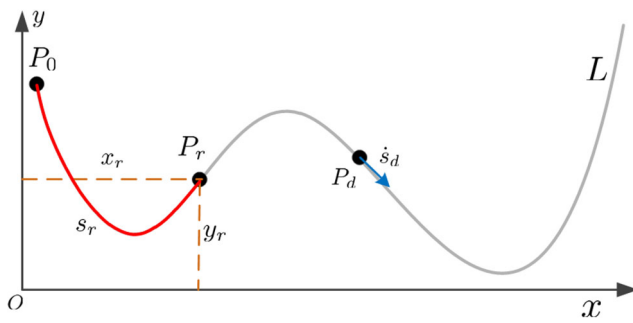


Fig. 1 The desired path with arc-length parameter s

$h_i(\delta_{xi}, \delta_{yi})$ of the structure relative to the center. Then, the desired path of each vehicle, $L_i(x_{di}, y_{di})$, is given by

$$L_i(s_i) = L(s_0) + R(\chi_0)h_i(\delta_{xi}, \delta_{yi}) \quad (2)$$

where

$$R(\chi_0) = \begin{bmatrix} \cos \chi_0 & \sin \chi_0 \\ -\sin \chi_0 & \cos \chi_0 \end{bmatrix} \quad (3)$$

is the rotation matrix from the Frenet-Serret frame to the inertial frame.

2.2 Control Objective

The main objective is to design a control scheme that exports the UAVs cooperative path following while ensuring a safe distance d_s between two UAVs. The cooperative path following is to ensure that the n vehicles move along the desired path and maintains a predefined structure such that

$$\begin{aligned} \lim_{t \rightarrow \infty} \|x_i - x_{di}\| &= 0 \\ \lim_{t \rightarrow \infty} \|y_i - y_{di}\| &= 0 \\ \lim_{t \rightarrow \infty} \|\chi_i - \chi_{di}\| &= 0 \\ \lim_{t \rightarrow \infty} \|s_i - s_d\| &= 0 \end{aligned} \quad (4)$$

Without losing generalisation, we propose a safe region, Ω_s , to indicate the relationship of them, i.e.

$$\Omega_s = \{P : P \in \mathbb{R}^2, \|P_i - P_j\| \leq d_s\} \quad (5)$$

where, P_i and P_j represent the position of UAV i and j , respectively. The definition of conflict region, Ω_c , is given by

$$\Omega_c = \{P : P \in \mathbb{R}^2, d_s \leq \|P_i - P_j\| \leq d_c\} \quad (6)$$

where $d_c > d_s$ is the distance that one vehicle closes to the other vehicle and collision avoidance will begin to work in the control effects. In addition, note that the safe region and the conflict region are the same for each vehicle.

The objective of collision avoidance operations is to guarantee that each UAV would not enter the other UAVs' safe region, while entering their conflict regions are allowed.

3 Control Scheme

In order to achieve the objective (4), a hybrid control scheme is proposed.

$$u_i = u_i^p + u_i^a \quad (7)$$

where, $u_i^p = [v_{gi}, \omega_i]^T$ indicates the control law satisfying cooperative path following, u_i^a represents the avoidance control devised to guarantee collision avoidance. We assume that a proper inner loop controller is well developed and it will track the commanded velocity v_{gi} and the heading angular velocity ω_i .

3.1 Cooperative Path Following

The error dynamical model is defined as

$$\begin{bmatrix} x_{ei} \\ y_{ei} \\ \chi_{ei} \end{bmatrix} = \begin{bmatrix} \cos \chi_i & \sin \chi_i & 0 \\ -\sin \chi_i & \cos \chi_i & 0 \\ 0 & 0 & 1 \end{bmatrix} \begin{bmatrix} x_i - x_{di} \\ y_i - y_{di} \\ \chi_i - \chi_{di} \end{bmatrix} \quad (8)$$

where χ_{di} indicates the path angle with respect to the desired point. The differential of Eq. 8 can be described by the path parameter s .

$$\begin{aligned} \dot{x}_{ei} &= v_{gi} - v_{di} \cos \chi_{ei} + y_{ei} \omega_i \\ \dot{y}_{ei} &= v_{di} \sin \chi_{ei} - x_{ei} \omega_i \\ \dot{\chi}_{ei} &= \omega_i - \omega_{di} \end{aligned} \quad (9)$$

where

$$\begin{aligned} v_{di} &= \sqrt{\dot{x}_{di}(s_i)^2 + \dot{y}_{di}(s_i)^2} \dot{s}_i = \hat{v}_{di}(s_i) \dot{s}_i \\ \omega_{di} &= \frac{\dot{x}_{di}(s_i) \dot{y}_{di}(s_i)^2 - \dot{x}_{di}(s_i)^2 \dot{y}_{di}(s_i)}{\dot{x}_{di}(s_i)^2 + \dot{y}_{di}(s_i)^2} \dot{s}_i = \hat{\omega}_{di}(s_i) \dot{s}_i \end{aligned} \quad (10)$$

The objective of the cooperative path following strategy is to drive $e_i = [x_{ei}, y_{ei}, \chi_{ei}]$ of each vehicle to $[0, 0, 0]$. Such that the UAVs employ their own positions to eliminate the tracking error to a predefined path and the position of each other to keep cooperative moving.

From Eq. 9, it is clear that control inputs of each vehicle include the ground speed v_{gi} , the rate of heading angle ω_i and the velocity of virtual vehicle \dot{s}_i (a ghost vehicle on the desired path).

Remark 1 The virtual vehicle is different to the center of the formation. As shown in Fig. 2, the center of four UAVs (1-4) is UAV 0 (UAV 0 is a virtual aircraft introduced here for computational convenience). For example, when UAV 1 approaches the desired path, a ghost vehicle, UAV 1', moves along the path from beginning to end. Due to the ghost vehicle being designed to fly exactly along the path. It just likes a ring encircles the path and only moving forward is allowed (in Fig. 1). The velocity of the ghost vehicle is \dot{s} , which is significant to influence the position of the vehicle

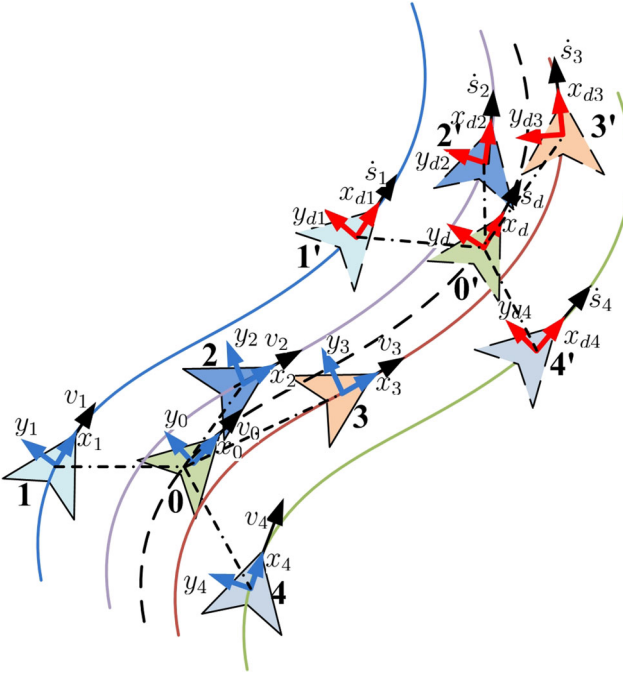


Fig. 2 The ghost vehicles on the paths

on the path. The center of the formation (UAV 0) also has a ghost vehicle (UAV 0') on the path.

When a group of UAVs are following their paths, the center of the formation is also pursuing a desired path $O_d(s_d) = (x_d(s_d), y_d(s_d))$, where s_d is the arc-length parameter, and \dot{s}_d is the velocity of the ghost vehicle of the center of the formation. Define $x_{e0} = x_d - x_0$, $y_{e0} = y_d - y_0$, and $E = \sqrt{x_{e0}^2 + y_{e0}^2}$ is the tracking error of the center of the formation. At this point, a proper \dot{s}_d is designed as

$$\dot{s}_d = \dot{s}_{d0} - v_s \frac{e^{k_e E} - 1}{e^{k_e E} + 1} \quad (11)$$

where, \dot{s}_{d0} is a basic velocity, $v_s \in (0, \dot{s}_{d0}]$ is a constant velocity and $k_e > 0$ is a control parameter. It is clear that the velocity of the ghost is directed toward maximum when the value of E is small and is toward minimum when E is large.

Theorem 1 Consider the error dynamical model defined in Eq. 9. Define the ghost vehicle of the center of the formation as Eq. 11. Suppose that the desired path of each vehicle, L_i , is parameterized via arc-length parameter s_i . Define control parameters $k_{\chi i} > 0$, then the control inputs

$$\begin{aligned} \omega_i &= -k_{\chi i} \chi_{ei} + \hat{\omega}_{di}(s_i) \dot{s}_d - y_{ei} \hat{v}_{di}(s_i) \dot{s}_d \frac{\sin \chi_{ei}}{\chi_{ei}} \\ \Theta &= \tilde{s}_i - x_{ei} \hat{v}_{di}(s_i) \cos \chi_{ei} + y_{ei} \hat{v}_{di}(s_i) \sin \chi_{ei} - \chi_{ei} \hat{v}_{di}(s_i) \\ \dot{s}_i &= \dot{\tilde{s}}_i + \dot{\tilde{s}}_i = -k_{si} \sin \Theta + \dot{s}_{d0} - v_s(t) \frac{e^{k_e E} - 1}{e^{k_e E} + 1} \\ v_{gi} &= -k_{xi} x_{ei} + \hat{v}_{di}(s_i) \dot{s}_i \cos \chi_{ei} \end{aligned} \quad (12)$$

drive x_{ei} , y_{ei} and χ_{ei} asymptotically to zero.

Proof The proof consists of two segments. First, the system asymptotically approaches the position of x axis with proposed control of v_{gi} . Then, we show that the virtual control value of \dot{s}_i asymptotically approaches \dot{s}_i and y_{ei} , χ_{ei} converge to zero simultaneously.

When design a control input to drive x_{ei} to zero, the variables \dot{s}_i should be retained as an additional input of each vehicle. On the basis of v_{gi} , we can conclude that

$$\begin{aligned} \dot{x}_{ei} &= -k_{xi} x_{ei} - (\hat{v}_{di}(s_i) \dot{s}_i - \hat{v}_{di}(s_i) \dot{s}_i \cos \chi_{ei}) + y_{ei} \omega_i \\ &= -k_{xi} x_{ei} - \hat{v}_{di}(s_i) \dot{s}_i \cos \chi_{ei} + y_{ei} \omega_i \end{aligned} \quad (13)$$

where, $\tilde{s}_i = \dot{s}_i - \dot{s}_i$ be the difference between actual value \dot{s}_i and virtual value of \dot{s}_i . It is clear that if \dot{s}_i and y_{ei} are zero, x_{ei} converges to zero. Meanwhile, $k_{xi} > 0$, \dot{s}_i is the virtual input of \dot{s}_i .

Consider the Lyapunov function candidate

$$V_1 = \frac{1}{2} \sum_{i=1}^n (x_{ei}^2 + y_{ei}^2 + \chi_{ei}^2 + (s_i - s_d)^2) \quad (14)$$

Differentiate the function to obtain

$$\begin{aligned} \dot{V}_1 &= \sum_{i=1}^n (x_{ei} \dot{x}_{ei} + y_{ei} \dot{y}_{ei} + \chi_{ei} \dot{\chi}_{ei} + (s_i - s_d)(\dot{s}_i - \dot{s}_d)) \\ &= \sum_{i=1}^n (-k_{xi} x_{ei}^2 - x_{ei} \hat{v}_{di}(s_i) \dot{s}_i \cos \chi_{ei} + x_{ei} y_{ei} \omega_i \\ &\quad + y_{ei} \hat{v}_{di}(s_i) \dot{s}_i \sin \chi_{ei} - x_{ei} y_{ei} \omega_i \\ &\quad + \chi_{ei}(\omega_i - \hat{\omega}_{di}(s_i) \dot{s}_i) + (s_i - s_d)(\dot{s}_i + \dot{s}_i - \dot{s}_d)) \\ &= \sum_{i=1}^n (-k_{xi} x_{ei}^2 - x_{ei} \hat{v}_{di}(s_i) \dot{s}_i \cos \chi_{ei} \\ &\quad + \chi_{ei} (y_{ei} \hat{v}_{di}(s_i) \dot{s}_i \frac{\sin \chi_{ei}}{\chi_{ei}} + \omega_i - \hat{\omega}_{di}(s_i) \dot{s}_i) \\ &\quad + (s_i - s_d)(\dot{s}_i + \dot{s}_i - \dot{s}_d)) \end{aligned} \quad (15)$$

If we select $\dot{s}_i = \dot{s}_d$, then we have

$$\begin{aligned} \dot{V}_1 &= \sum_{i=1}^n (-k_{xi} x_{ei}^2 + \chi_{ei} (y_{ei} \hat{v}_{di}(s_i) (\dot{s}_i + \dot{s}_i) \frac{\sin \chi_{ei}}{\chi_{ei}} \\ &\quad + \omega_i - \hat{\omega}_{di}(s_i) (\dot{s}_i + \dot{s}_i))) \\ &\quad + (s_i - s_d - x_{ei} \hat{v}_{di}(s_i) \cos \chi_{ei}) \dot{s}_i \\ &= \sum_{i=1}^n (-k_{xi} x_{ei}^2 + \chi_{ei} (y_{ei} \hat{v}_{di}(s_i) \dot{s}_i \frac{\sin \chi_{ei}}{\chi_{ei}} + \omega_i \\ &\quad - \hat{\omega}_{di}(s_i) \dot{s}_i) + \dot{s}_i (s_i - s_d - x_{ei} \hat{v}_{di}(s_i) \cos \chi_{ei} \\ &\quad + y_{ei} \hat{v}_{di}(s_i) \sin \chi_{ei} - \chi_{ei} \hat{v}_{di}(s_i))) \\ &= \sum_{i=1}^n (-k_{xi} x_{ei}^2 + \chi_{ei} (y_{ei} \hat{v}_{di}(s_i) \dot{s}_d \frac{\sin \chi_{ei}}{\chi_{ei}} + \omega_i \\ &\quad - \hat{\omega}_{di}(s_i) \dot{s}_d) + \dot{s}_i (\tilde{s}_i - x_{ei} \hat{v}_{di}(s_i) \cos \chi_{ei} \\ &\quad + y_{ei} \hat{v}_{di}(s_i) \sin \chi_{ei} - \chi_{ei} \hat{v}_{di}(s_i))) \end{aligned} \quad (16)$$

With the aid of Eq. 12, V_2 yields

$$\dot{V}_1 = \sum_{i=1}^n (-k_{xi}x_{ei}^2 - k_{\chi i}\chi_{ei}^2 - k_{si}\Theta \sin \Theta) \leq 0 \quad (17)$$

Applying Barbalat's lemma we can obtain

$$\begin{aligned} \lim_{t \rightarrow \infty} x_{ei} &\rightarrow 0 \\ \lim_{t \rightarrow \infty} \chi_{ei} &\rightarrow 0 \\ \lim_{t \rightarrow \infty} \Theta &\rightarrow 0 \end{aligned} \quad (18)$$

That is to say

$$\begin{aligned} \lim_{t \rightarrow \infty} (\tilde{s}_i - x_{ei}\hat{v}_{di}(s_i) \cos \chi_{ei} \\ + y_{ei}\hat{v}_{di}(s_i) \sin \chi_{ei} - \chi_{ei}\hat{v}_{di}(s_i)) &\rightarrow 0 \end{aligned} \quad (19)$$

and we can conclude

$$\lim_{t \rightarrow \infty} \tilde{s}_i \rightarrow 0 \quad (20)$$

If we substitute the control of ω_i in Eq. 12 into error dynamical model of χ_{ei} in Eq. 9, we can obtain

$$\dot{\chi}_{ei} = -k_{\chi i}\chi_{ei} - \hat{\omega}_{di}(s_i)\dot{\tilde{s}}_i - y_{ei}\hat{v}_{di}(s_i)\dot{s}_d \frac{\sin \chi_{ei}}{\chi_{ei}} \quad (21)$$

Since $\lim_{t \rightarrow \infty} \chi_{ei} \rightarrow 0$ and $\lim_{\chi_{ei} \rightarrow 0} \frac{\sin \chi_{ei}}{\chi_{ei}} \rightarrow 1$. According to Lemma 2 in [18], it is obvious that

$$\lim_{t \rightarrow \infty} y_{ei} \rightarrow 0 \quad (22)$$

which finishes the proof. \square

Remark 2 Specifically, the control input of ω_i in Eq. 12 may result in a singularity when $\chi_{ei} = 0$. Then, a transfer $\frac{\sin \chi_{ei}}{\chi_{ei}} = \int_0^1 \cos(\eta \chi_{et}) d\eta$ is introduced such that

$$\begin{aligned} \omega_i = -k_{\chi i}\chi_{ei} + \hat{\omega}_{di}(s_i)\dot{s}_d \\ - y_{ei}\hat{v}_{di}(s_i)\dot{s}_d \int_0^1 \cos(\eta \chi_{ei}) d\eta \end{aligned} \quad (23)$$

3.2 Collision Avoidance

The above cooperative path following control law applies to guarantee the tracking error of the UAVs converging to zero only. Collision of the vehicles may occur when the trajectories of the UAVs tend to cross. It is essential to develop collision avoidance method to ensure collision-free maneuvers. Notice that the collision avoidance control is silent most of the time and only active when the positions of UAVs are within the conflict region as defined in Eq. 6.

Small fixed-wing UAV often cruises to high speed (15–30 m/s) and it is difficult to implement collision avoidance maneuvers when the distance of the vehicles are close. Due to the fact that the UAVs are sensitive to wind disturbances, noise and uncertainties, collision avoidance actions must be implemented fast and efficiently. Once probable collisions have been determined, the avoidance method must drive

the vehicle toward an appropriate direction and follow the desired path to safety.

The method vector field histogram (VFH) was first proposed by [19]. This method employs the form of a window grid to define the distance between the vehicle and the obstacle in two-dimensional space. The vehicle is in the center of a rectangular grid and expresses the possibility of an obstacle to this grid by defining a certainty value (CV) for each cell in the sensor's detection range. A range α is defined to divide the polar coordinate into fractions. Then the two-dimensional grid information is converted into a polar histogram. CV matrix translates into polar obstacle density associated with each sector. The final direction and speed control output are obtained by selecting the appropriate threshold and target position.

Here, we improve the basic VFH method to fixed-wing UAV collision avoidance. A reachable set is defined based on the nose pointing and the maximum turning rate. As shown in Fig. 3, the red solid line represents the reachable set and the window grid is generated by a polar histogram, which has been divided into many cells and the CV, $cv_{i,j}$, is calculated according to the confidence of an obstacle for each cell. Finally, a CV matrix is obtained

$$\Gamma = \{cv_{i,j}\} \quad (24)$$

Take, for instance, the matrix in Fig. 3 is given by

$$\Gamma = \begin{bmatrix} 3 & 3 & 2 & 1 & 1 & 3 & 3 & 2 \\ 3 & 4 & 2 & 1 & 1 & 2 & 2 & 2 \\ 3 & 3 & 2 & 1 & 0 & 1 & 1 & 1 \\ 2 & 2 & 2 & 1 & 0 & 0 & 0 & 0 \\ 1 & 1 & 1 & 0 & 0 & 0 & 0 & 0 \end{bmatrix} \quad (25)$$

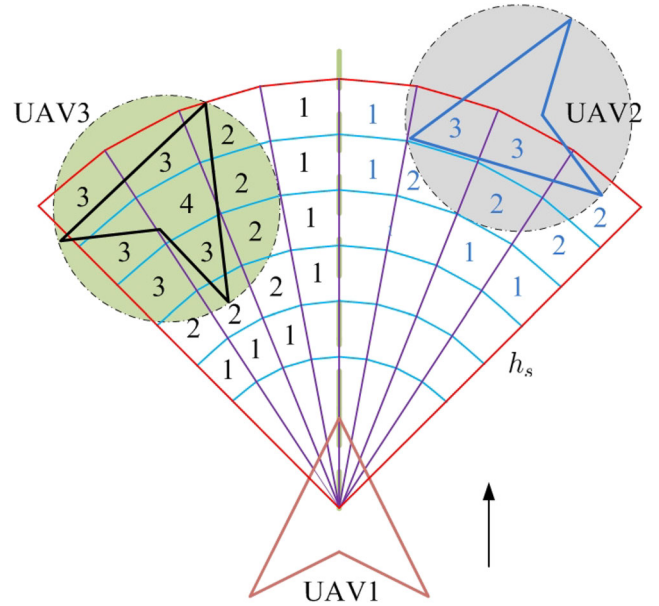
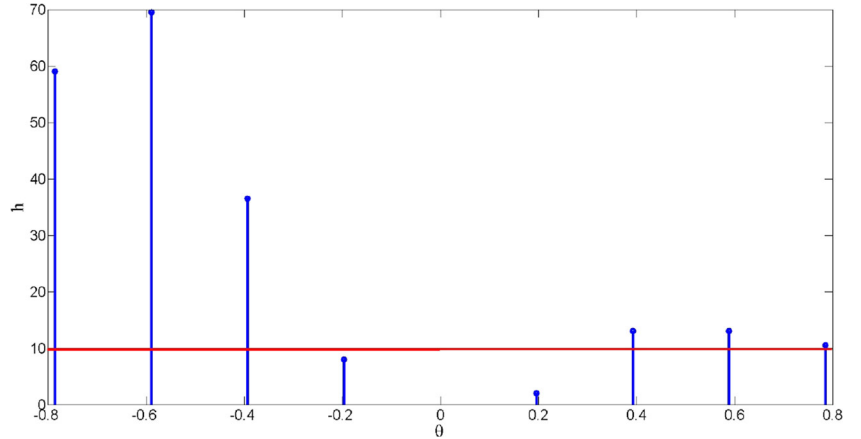


Fig. 3 The reachable set and certainty value of active cells

Fig. 4 Polar density of sectors

If the CV of a cell is nonzero, this cell is active. All the active cells form the outline of the obstacle. The closer to the center of the obstacle, the larger the CV is. This creates a lot of vectors pointing to the center of the obstacle. The direction of every active cell is defined as

$$\beta_{i,j} = \tan^{-1} \frac{y_i - y_0}{x_i - x_0} \quad (26)$$

and the magnitude is obtained

$$m_{i,j} = cv_{i,j}^2(h_s - d_{i,j}) \quad (27)$$

where:

$\beta_{i,j}$ Direction from the active cell to the center of the vehicle.

(x_i, y_i) The center of the active cell.

(x_0, y_0) The center of the vehicle.

h_s The maximum detection distance of the vehicle.

$d_{i,j}$ Distance from the active cell to the center of the vehicle.

By selecting a suitable size α , the polar histogram is divided into the same spacing. Each equi-partition corresponds to a certain direction of the sector k . Such that $\alpha * k = 2\rho_m$, where ρ_m is the maximum turn angle of the vehicle. In this paper, $\alpha = 5^\circ$, $\rho_m = 45^\circ$, i.e., there are

18 sectors. After summing each sector corresponds to the magnitude of the cells to calculate the polar obstacle density

$$den_k = \sum_{i,j} m_{i,j} \quad (28)$$

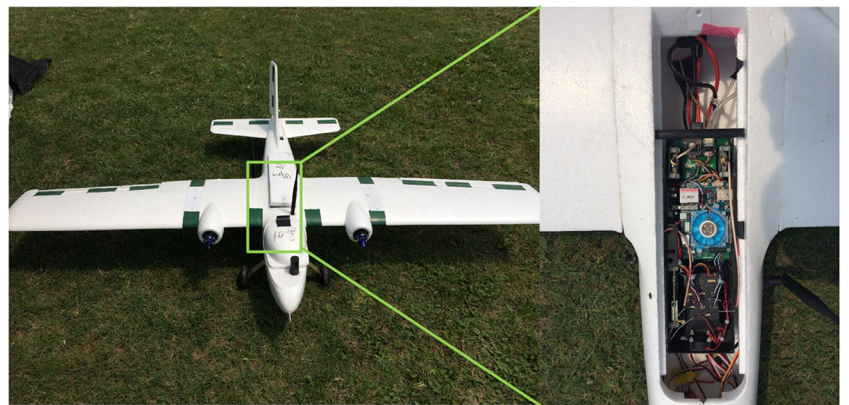
The polar density of Fig. 2 is shown in Fig. 4. In order to decrease the flutter of the sector, a smoothing function is introduced

$$den_k^* = \frac{\sum_{n=-l}^l h_{k-n}}{2l + 1} \quad (29)$$

where $l = 4$ is the size of window.

As shown in Fig. 4, a proper threshold ρ_h (red line) is applied to obtain the steering direction of the vehicle. Valleys (obstacle densities below the threshold) can be used as a candidate and the one that approach the desired path is selected. The center of the selected valley is the avoidance direction of the vehicle. While, the speed of the aircraft needs to be within the maximum v_{\max} and minimum v_{\min} speed range at all times. When there is an obstacle in front of the vehicle, it needs to slow down properly. This reduction in speed is calculated by the function

$$v_{a,i} = (v_{\max} - v_{\min}) * (1 - h_k^*/h_m) + v_{\min} \quad (30)$$

Fig. 5 The fixed-wing UAV for the real flight test

where, h_k^* represents the obstacle density of the direction θ_f , h_m is a constant that is particularly chosen to meet the reduction in velocity.

Algorithm 1 VFH method for collision avoidance.

```

1: Initialize:  $h_s$ ,  $h_m$ ,  $\rho_m$ ,  $d_c$ ,  $d_s$ ,  $\rho_h$  and  $\alpha$ ;
2: Obtain the state of UAV:  $[(x_0, y_0), \chi]$ ;
3: Obtain the positions of obstacle and other vehicles in a group:  $[(x_{ob}, y_{ob})]$  and  $[(x_j, y_j)]$ ;
4: Calculate the distance  $d_{ij}$  from the vehicle  $(x_0, y_0)$  to obstacle  $[(x_{ob}, y_{ob})]$  and other vehicles  $(x_j, y_j)$ ;
5: if  $d_{ij} > d_c$ , No collision detected; then
6:   break;
7: end if
8: if  $d_{ij} < d_s$ , Emergency; then
9:   landing;
10: end if
11: if  $d_c \geq d_{ij} \geq d_s$  then
12:    $k \Leftarrow 2\rho_m/\alpha$ ;
13:   Set the certainty value (CV) for each cell;
14:   Obtain the CV matrix  $\Gamma$ ;
15:   Calculate the magnitude  $m_{i,j}$  of each active cell by Eq. 27;
16:   Calculate the polar obstacle density  $den_k^*$  for each sector by Eqs. 28 and 29;
17: end if
18: if No valley detected; then
19:   repeat
20:      $\rho_h \Leftarrow \rho_h * 1.5$ ;
21:   until valley detected;
22: end if
23: Select a valley that closed to the desired path and calculate the center of this valley,  $\theta_f$ ;
24: Calculate the speed of the vehicle  $v_{a,i}$  by Eq. 30;
25: The avoidance maneuvers of the heading of the vehicle is given by  $[v_f, \omega_f]$ .

```

Define the distance between the UAV i and the UAV j as dis_{ij} . We propose the following collision avoidance control law

$$u_i^a = -K_a u_i^p + [v_f, \omega_f]^T \quad (31)$$

where $\omega_f = \theta_f - \chi$ is the heading avoidance maneuver, $v_f = v_{a,i}$ is the velocity avoidance maneuver. K_a , the path loss factor, is given by

$$K_a = \begin{cases} 1, & \text{if } dis_{ij} \leq d_s \\ \frac{\sqrt{d_c^2 - dis_{ij}^2}}{\sqrt{dis_{ij}^2 - d_s^2} \sqrt{d_c^2 - d_s^2}}, & \text{otherwise} \\ 0, & \text{if } dis_{ij} \geq d_c \end{cases} \quad (32)$$

4 Experiment

4.1 Experiment Setup

The cooperative curved path following method with collision avoidance proposed in Section 3 is validated via

With the previous description as foundation, the collision avoidance algorithm is summarized in Algorithm 1.

real flight tests of fixed-wing UAV. As shown in Fig. 5, all vehicles use the same configuration and size. The wingspan of the vehicle is 1800 mm, body length is 1220 mm, the whole weight is 1.1 kg, the maximum take-off weight is 5 kg, cruising speed is 17 m/s, and the flight altitude is 100–200 m.

All flight tests are carried out based on semi-physical simulation tests [20, 21]. The electrical diagram of the entire onboard module as shown in the Fig. 6, the host computer and the autopilot (Pixhawk) communicate by agreement. We use the proven commercial Pixhawk autopilot as the underlying flight control element. The status and position information of the vehicle are obtained via sensors and being sent to the host computer. The cooperative curved path following method is implemented on the host computer that runs Ubuntu 14 as the operating system, which solves the required altitude, the desired speed and the desired heading according to the current state information and the expected path direction. The information is then sent to the autopilot through the communication protocol. The autopilot uses its own control algorithm (feed forward and PID controller) to

Fig. 6 Onboard connection diagram

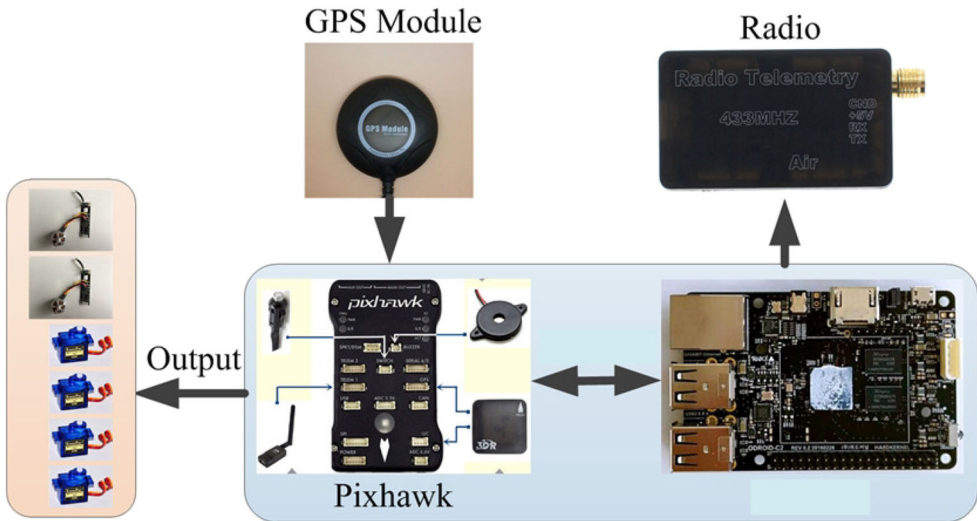


Table 1 Cooperative control parameters and obstacle avoidance parameters

Cooperative control parameters		Obstacle avoidance parameters	
Parameter	Value	Parameter	Value
$k_{\chi i}$	1.5	h_m	10
k_{ei}	1.2	h_s	100
k_{si}	0.5	ρ_m	45°
k_e	0.1	d_c	20 m
k_{xi}	0.2	d_s	10 m
		ρ_h	10
		l	4
		α	5°

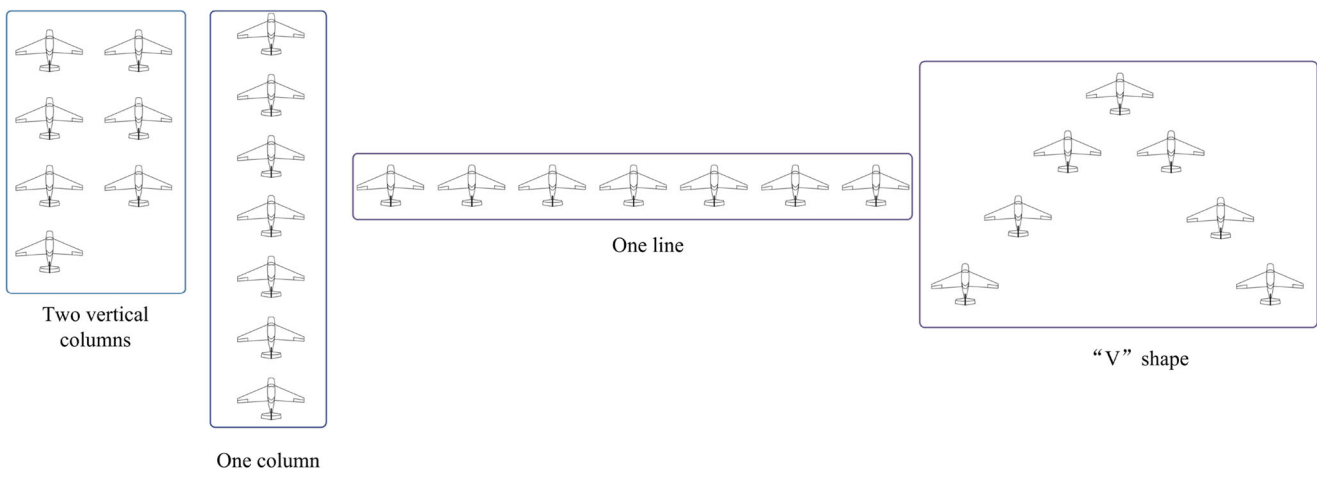


Fig. 7 Four different formations

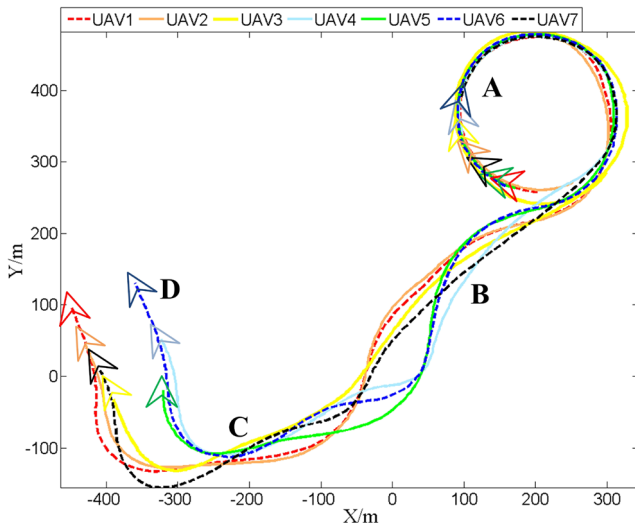


Fig. 8 All aircraft began to fly together after they rallied

obtain the actual control output and send it directly to the actuator (motor and steering gear).

In order to verify the validity and practicability of the proposed algorithm, we use 21 vehicles cooperative flight tests. The vehicles were divided into three clusters, with seven aircraft and one virtual center in each cluster. When performing cooperative tasks, not only the aircraft in the cluster will coordinate the path following, but also the coordination of the relative positions of virtual clusters in each cluster. In order to draw a clear picture, we use a cluster of 7 aircraft to display the experimental results. Due to the limitation of the flight environment and communication distance, we use the square loop route as the basic flight

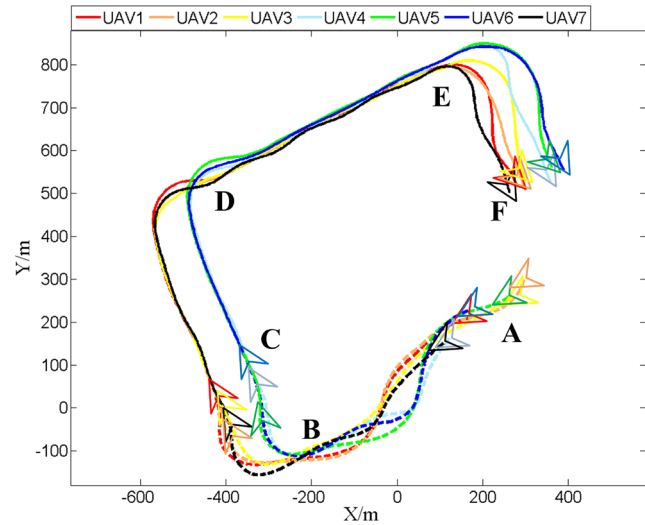


Fig. 10 Within a cluster, the vehicles changed from “Two vertical columns” to “One column”

path. On this basis, in order to better achieve multi-aircraft coordination and formation transformation, the desired path of all aircraft is a planned curve path. The curve ensures that the vehicle can smoothly transition both inside and outside of the formation during turning and formation transformation.

4.2 Paramater Setup

The parameters used in our proposed method are divided into two parts: cooperative control parameters and obstacle avoidance parameters. The values of each parameter are shown in Table 1.

Fig. 9 In the first phase, the yaw (degree) and airspeed (m/s) of all aircraft

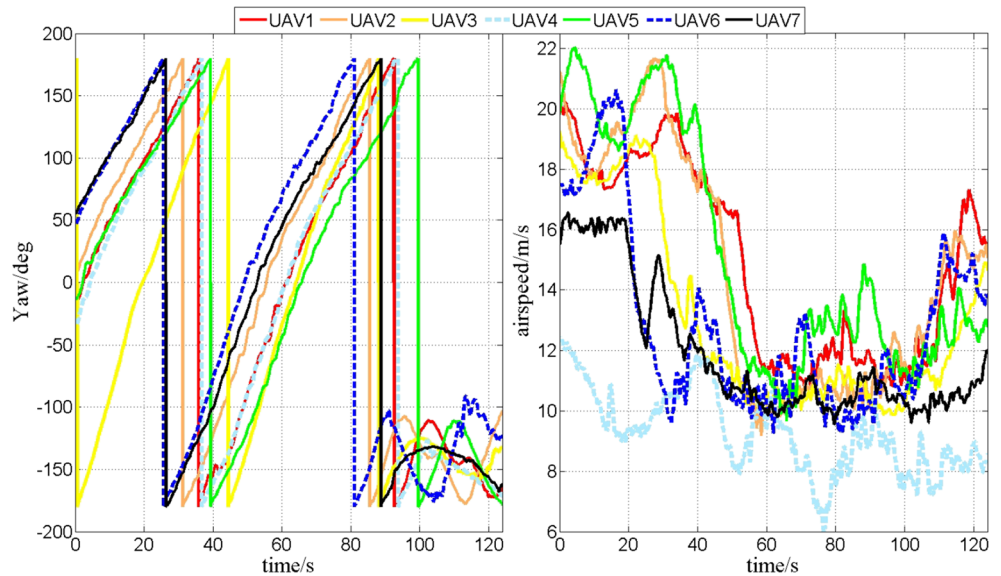
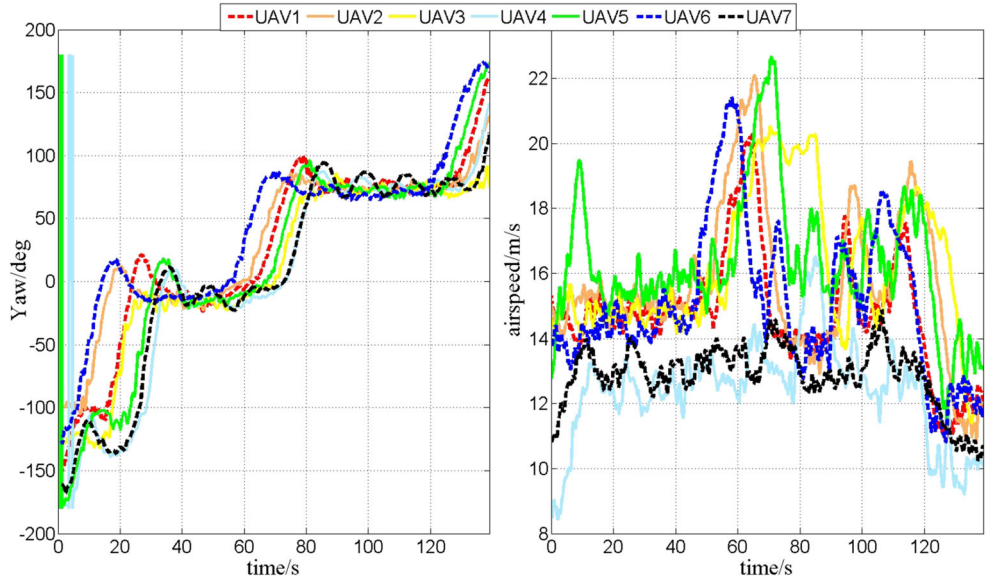


Fig. 11 In the second phase, the yaw (degree) and airspeed (m/s) of all aircraft



4.3 Formation Type

To better verify the effectiveness of the proposed method in flight experiments, we designed four different formations (two vertical columns, one column, one line, “V” shape). A simple schematic of each formation is shown in the Fig. 7.

4.4 Results

All aircraft take off on the runway in two rows. Due to the limitations of the take off order, vehicles that took off first need to circle in the air after the other aircraft in the same cluster are taking off. As shown in Fig. 8, all vehicles began to fly together after completing the hovering at point A. After the adjustment at point B, coordinated path tracking starts at point C. At D, the aircraft is divided into two teams, each of which is a column flight. The yaw and airspeed of all vehicles are shown in Fig. 9.

As shown in Fig. 10, the aircraft began its coordinated flight at point A and turned into “Two vertical columns” at point B. When passing through points B, C, and D, the UAVs maintained the formation of “Two vertical columns”. At point D, the formation is transformed into “One column”. Finally, from point E to point F, the formation changes to “One line”. The yaw and airspeed of all vehicles are shown in Fig. 11.

Point A and point B in Fig. 12 correspond to point D and point E in Fig. 10, respectively. In Fig. 12, the aircraft keep the “One line” formation from point B to point C, and transform to “V” shape in position D and E after cross-

cutting. The yaw and airspeed of all vehicles are shown in Fig. 13.

It is worthwhile to mention that a real anti-collision test is difficult to complete with a real aircraft. We use a virtual target for the desired path to guide the vehicle to avoid this virtual intruder. Although some of the expected paths of the aircraft cross in the process of cooperative path following, the collision avoidance algorithm effectively guarantees the safe flight of all the aircraft. To be able to better test the effectiveness of the proposed collision avoidance algorithm, we added a virtual obstacle to the desired flight path. Based on its own position and the

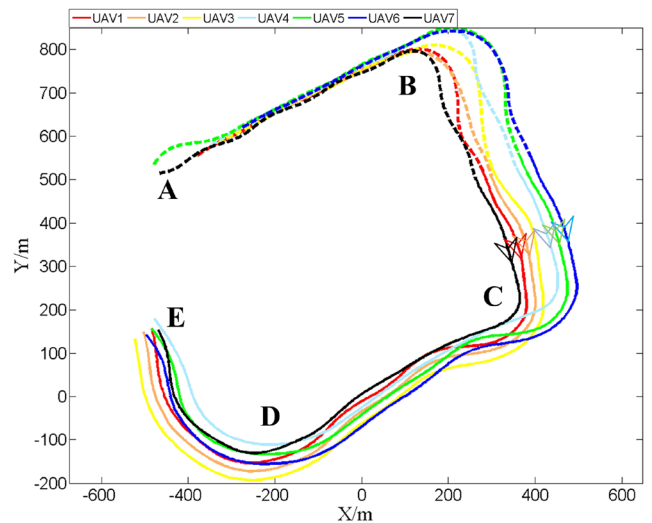
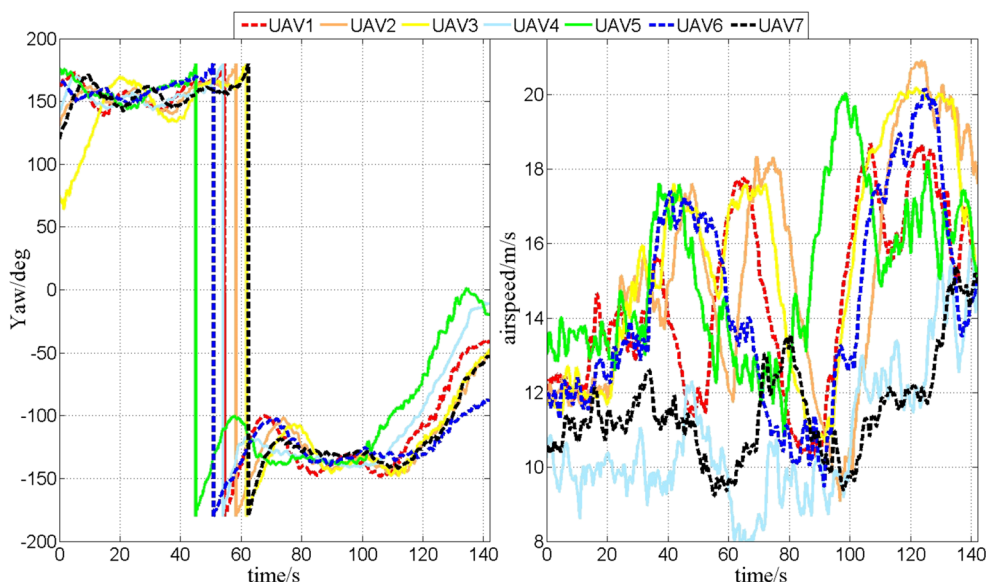


Fig. 12 The vehicles from “One column” into a “V” shape

Fig. 13 In the third phase, the yaw (degree) and airspeed (m/s) of all aircraft



distance from the obstacle, the aircraft made a reasonable avoidance action in conjunction with Algorithm 1. As shown in Fig. 14, the brown circle represents the obstacle, just above the desired path. When the aircraft approaches the obstacle gradually, path following control output fails and the collision avoidance control output is used. When the aircraft is still tracking in the normal path from point A to point B, and gradually approaches the obstacle from point B to point C, the path following control output fails and adopts collision avoidance control output. After reaching point D, the collision avoidance output will continue to return to the

path following output. The yaw and airspeed of all vehicles are shown in Fig. 15.

There are many other experiments that have been carried out in varying environments, e.g., with different wind and temperature. The hybrid cooperative path following method successfully navigated a group of vehicles for their desired path to all cases. Due to limited space, the results of these experiments will not be repeated.

5 Conclusion

In this paper we discussed a cooperative curved path following strategy that integrates a virtual structure, a kinematic model based method, and a collision avoidance method to ensure collision-free maneuvers for a group of UAVs cooperatively flying in alterable formation. In most fixed-wing UAV collaborative control processes, the vehicle is assumed to move at a constant velocity and then accomplish the cooperative task by adjusting the heading. But this will make the time taken to accomplish the cooperative task increase, while the vehicles are more prone to collision in the path following. In order to obtain a fast cooperative path following algorithm, a hybrid control scheme, integrated with both a virtual structure and a kinematic model is proposed, and an additional “freedom of velocity” control s is considered explicitly. According to the basic vector field histogram (VFH) algorithm, a safe and efficient collision avoidance algorithm is introduced. Real flight tests with small fixed-wing UAVs are developed to verify the effectiveness and applicability of the proposed control strategy.

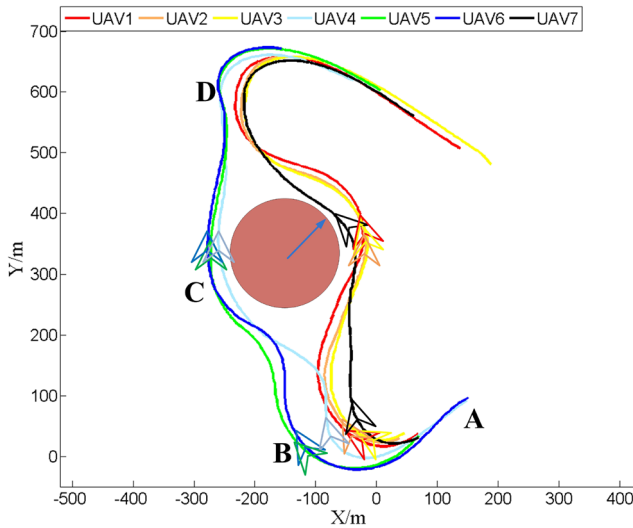
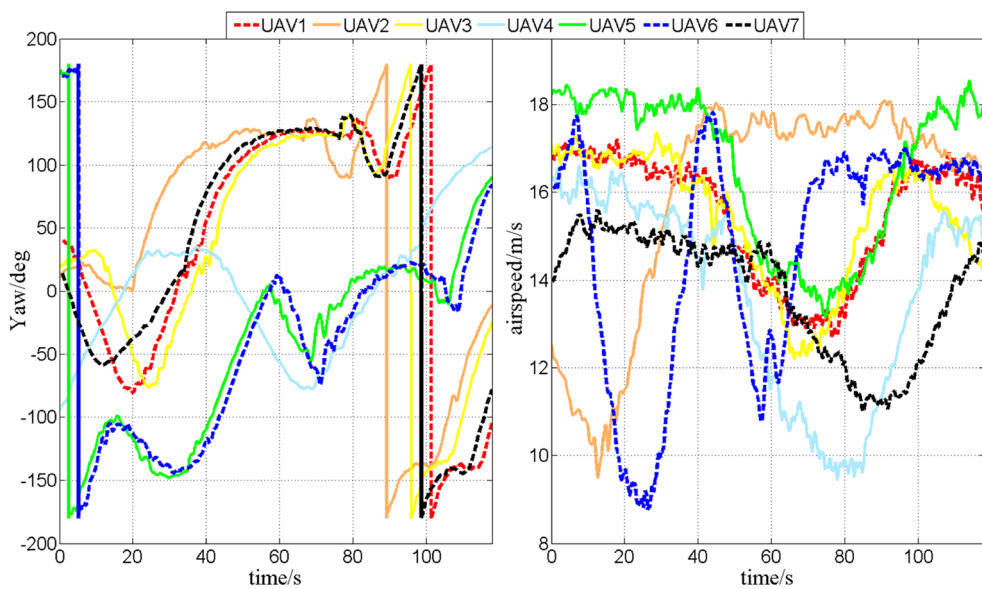


Fig. 14 The aircraft continued to follow the path after bypassing the obstacle

Fig. 15 In the collision avoidance phase, the yaw (degree) and airspeed (m/s) of all aircraft



References

- Wang, X., Yadav, V., Balakrishnan, S.N.: Cooperative uav formation flying with obstacle/collision avoidance. *IEEE Trans. Control Syst. Technol.* **15**(4), 672–679 (2007)
- Patil, S., van, J., Alterovitz, R.: Estimating probability of collision for safe planning under gaussian motion and sensing uncertainty. In: Proceedings of the IEEE International Conference on Robotics and Automation, pp. 3238–3244 (2012)
- Richards, A., How, J.: Decentralized model predictive control of cooperating uavs. In: IEEE Conference on Decision and Control, pp. 3238–3244 (2005)
- Sathyaraj, B.M., Jain, L.C., Finn, A., S. Drake.: Multiple uavs path planning algorithms: a comparative study. *Fuzzy Optim. Decis. Making* **7**(3), 257–267 (2008)
- Koenig, S., Likhachev, M.: Fast replanning for navigation in unknown terrain. *IEEE Trans. Robot.* **21**(3), 354–363 (2005)
- Abichandani, P., Ford, G., Benson, H.Y., Kam, M.: Mathematical programming for multi-vehicle motion planning problems. In: Proceedings of the IEEE International Conference on Robotics and Automation, pp. 3315–3322 (2012)
- Besada-Portas, E., Torre, L., Cruz, J.M., Andres-Toro, B.: Evolutionary trajectory planner for multiple uavs in realistic scenarios. *IEEE Trans. Robot.* **26**(4), 619–634 (2010)
- Alejo, D., Cobano, J.A., Heredia, G., Ollero, A.: Collision-free 4d trajectory planning in unmanned aerial vehicles for assembly and structure construction. *J. Intell. Robot. Syst.* **73**(1), 783–795 (2014)
- Ge, S.S., Cui, Y.J.: New potential functions for mobile robot path planning. *IEEE Trans. Robot. Autom.* **16**(5), 615–620 (2000)
- Matveev, A.S., Teimoori, H., Savkin, A.V.: A method for guidance and control of an autonomous vehicle in problems of border patrolling and obstacle avoidance. *Automatica* **47**(3), 505–514 (2011)
- Matveev, A.S., Hoy, M., Savkin, A.V.: The problem of boundary following by a unicycle-like robot with rigidly mounted sensors. *Robot. Auton. Syst.* **61**(3), 312–327 (2013)
- Huang, L.: Wall-following control of an infrared sensors guided wheeled mobile robot. *Int. J. Intell. Sys.* **7**(1), 106–117 (2009)
- Lan, Y., Yan, G., Lin, Z.: Synthesis of distributed control of coordinated path following based on hybrid approach. *IEEE Trans. Autom. Control* **56**(5), 1170–1175 (2011)
- Beard, R.W., Ferrin, J., Humphreys, J.: Fixed wing uav path following in wind with input constraints. *IEEE Trans. Control Syst. Technol.* **22**(6), 2103–2117 (2014)
- Fukushima, H., Kon, K., Matsuno, F.: Distributed model predictive control for multi-vehicle formation with collision avoidance constraints. In: Proceedings of the 44th IEEE Conference on Decision and Control, pp. 5480–5485 (2005)
- Nelson, D.R., Barber, D.B., McLain, T.W., Beard, R.W.: Vector field path following for miniature air vehicles. *IEEE Trans. Robot.* **23**(3), 519–529 (2007)
- Aguiar, A., Hespanha, J., Kokotovic, P.: Performance limitations in reference tracking and path following for nonlinear systems. *Automatica* **44**(3), 598–610 (2008)
- Jiang, Z.P., Nijmeijer, H.: Tracking control of mobile robots : a case study in backstepping. *Automatica* **33**(1), 1393–1399 (1997)
- Borenstein, J., Koren, Y.: The vector field histogram-fast obstacle avoidance for mobile robots. *IEEE Trans. Robotics Automation* **7**(3), 278–288 (1991)
- Zhao, S., Wang, X., Zhang, D., Shen, L.: Curved path following control for fixed-wing unmanned aerial vehicles with control constraint. *J. Intell. Robot. Syst.* **89**(1-2), 107–119 (2018)
- Zhao, S., Wang, X., Zhang, D., Shen, L.: Model-free fuzzy adaptive control of the heading angle of fixed-wing unmanned aerial vehicles. *Journal of Aerospace Engineering* **30**(4) (2017)

Publisher's Note Springer Nature remains neutral with regard to jurisdictional claims in published maps and institutional affiliations.

Shulong Zhao received the B.S. degrees from Beihang University (BUAA), China in 2011, and received the M.S. and Ph.D. degrees from National University of Defense Technology (NUDT), China in 2014 and 2017, respectively. Currently he is a lecturer of College of Intelligence Science and Technology, National University of Defense Technology. His research interests include data driven control, and curved path following of UAV.

Xiangke Wang received the B.S., M.S., and Ph.D. degrees from National University of Defense Technology, China, in 2004, 2006 and 2012, respectively. From 2012, he is with College of Intelligence Science and Technology, National University of Defense Technology, China, and currently he is an professor there. His current research interests include coordination control of multiple UAV, nonlinear control of UAV.

Hao Chen received his Bachelor of Engineering (2013) and Master of Engineering (2015) from National University of Defense Technology (NUDT), where he is currently working toward the Ph.D. degree. The focus of his research lies on multi-UAV coordination.

Yajing Wang received the B.S. and M.S. degrees from College of Intelligence Science and Technology, National University of Defense Technology, China, in 2016 and 2018, respectively, and currently she is a Ph.D. student there. Her current research interests include collision avoidance of multiple UAVs, distributed optimization control for nonlinear uncertain systems.